Spectroscopy of Jet-Cooled Bi_3†

Caleb A. Arrington‡ and Michael D. Morse*

Department of Chemistry, University of Utah, Salt Lake City, Utah 84112

Received: July 21, 2008; Revised Manuscript Received: September 16, 2008

A resonant two-photon ionization spectroscopic study of jet-cooled Bi_3 has identified two band systems in the molecule in the 9600−10 600 and 15 250−16 050 cm^{-1} range. The latter of these has been previously observed in matrix isolation spectroscopy and tentatively attributed to Bi_4; the mass-resolved work presented here reassigns it to Bi_3. A review of all previously observed electronic states is presented, and it is argued that the new band system lying in the range 9600−10 600 cm^{-1} corresponds to the spin-forbidden $\tilde{A}'\ ^4A_1'' \leftarrow \tilde{X}_1\ ^2E''$ ($E_{1/2}$ component) band system.

I. Introduction

The group 15 dimers, N_2, P_2, As_2, Sb_2, and Bi_2, are all stable molecules in the gas phase, existing as either the most abundant gaseous form of the element or as a readily produced molecule in the high temperature vapors above the solid or molten element. These molecules all have $X\ ^1\Sigma_g^+$ ground states with a formal triple bond, and the ground and excited states are spectroscopically very well characterized.[1] Most of the mixed group 15 diatomics are spectroscopically known as well with well-established $X\ ^1\Sigma^+$ ground states and with vibrational frequencies and bond lengths accurately known for PN,[2−4] AsN,[5,6] SbN,[7−9] BiN,[10,11] AsP,[12,13] SbP,[7,14] BiP,[10,15,16] and BiAs.[15,16] Only for SbAs and BiSb are measurements of the ground-state bond length currently unavailable.

The triatomic clusters, apart from N_3, are not so well known. The N_3 molecule has been known since 1956 as a linear molecule with an $\tilde{X}\ ^2\Pi_g$ ground state,[17] and numerous detailed investigations have been made subsequent to its discovery.[18−21] The ground states of the remaining trimers have all been calculated to derive from $^2E''$ ground states in D_{3h} geometry.[22,23] Such orbitally degenerate states are subject to Jahn−Teller distortion, splitting into $^2A_2$ and $^2B_1$ forms in C_{2v} geometry. The potential energy minima of these surfaces correspond to obtuse ($\theta > 60°$) and acute ($\theta < 60°$) isosceles triangles, respectively.[22,23] The Jahn−Teller splitting in these molecules is calculated to be small, with the $^2A_2$ and $^2B_1$ states lying within 0.06 eV (480 cm^{-1}) of each other, regardless of whether the molecule is P_3, As_3, Sb_3, or Bi_3.[22,23] The deviations from the equilateral structure are also predicted to be small, with the $^2A_2$ states having the unique angle of the isosceles triangle lying in the range of 64.2−66.7°, while the $^2B_1$ states have the unique angle lying in the range of 55.0−56.3°.[22,23]

Spectroscopic investigations of the group 15 trimers are very limited, apart from N_3. An electronic band system near 427 nm, assigned to P_3, has been observed in cryogenic argon matrices.[24] Investigations of the group 15 trimers using photodetachment spectroscopy of mass-selected cluster anions have been conducted for P_n^- (n = 1−9),[25] As_n^- (n = 1−5),[26] Sb_n^- (n = 1−9),[27,28] and Bi_n^- (n = 2−21).[28,29] Although the resulting photoelectron spectra display resolved vibrational structure for the diatomic molecules and for P_3^-,[25−27,29] the spectra of the remaining trimers and larger clusters only contain electronic information.

More information is known about the tetrahedral tetramers P_4,[30−33] As_4,[34−37] and Sb_4.[38,39] For these elements, the thermodynamically favored species at low temperatures in the gas phase is the tetramer, which belongs to the tetrahedral point group, T_d. In the case of bismuth, a number of band systems observed in matrix isolation investigations have been tentatively assigned to the Bi_4 molecule.[40−44] Our original motivation for this work was to study these band systems in the gas phase, but in the process we have determined that they originate from Bi_3, instead of Bi_4. Our reassignment of the carrier of the spectrum has been greatly assisted by the use of a mass-sensitive detection method: resonant two-photon ionization (R2PI) spectroscopy with detection of the ions produced in a time-of-flight mass spectrometer. To our knowledge, this constitutes the only gas phase optical study of a group 15 trimer, apart from N_3.

Bismuth has the largest nuclear charge, $Z = 83$, of all of the stable elements. The high nuclear charge of this atom causes electrons that penetrate close to the nucleus to develop velocities that approach the speed of light. Thus, relativistic effects are of critical importance in understanding the chemistry of bismuth, and bismuth compounds provide an important test of relativistic quantum chemical methodologies. The relativistic increase in mass that occurs when a particle moves at speeds approaching the speed of light leads to a contraction in atomic orbital sizes, owing to the inverse dependence of the atomic scale of length, the Bohr radius, on the mass of the electron. Thus, orbitals that penetrate close to the nucleus are contracted and stabilized by relativistic effects. This phenomenon is quite significant in bismuth, where a comparison of a relativistic Dirac−Fock calculation to a nonrelativistic Hartree−Fock calculation shows that the 6s orbital contracts by about 12% when relativistic effects are included.[45] Likewise, the binding energy calculated for the 6s electron in a Dirac−Fock calculation is 3.5 eV greater than that calculated in the nonrelativistic Hartree−Fock method.[45] As a result, while it is relatively easy to remove the 6p electrons and leave bismuth in a Bi^{3+} charge state, further oxidation to produce a Bi^{5+} ion by removal of the two 6s electrons is severely hampered by the relativistic stabilization of these electrons. Throughout the 6p block, this stabilization

† Part of the "Karl Freed Festschrift".

* To whom correspondence should be addressed. E-mail: morse@chem.utah.edu.

‡ Present address: Wofford College, 429 North Church Street, Spartanburg, SC 29303-3663.

10.1021/jp806436n CCC: $40.75
Published on Web 11/12/2008

of the 6s electrons has been termed the "inert pair effect" and is well-known to inorganic chemists.[46]

Another relativistic effect that is of paramount importance in bismuth is the spin−orbit interaction. It is well known that the orbital spin−orbit parameter, $\zeta_{n\ell}$, increases substantially as the nuclear charge, Z, increases. For the valence 6p orbitals of bismuth, however, ζ_{6p} is so large (about 10 100 cm^{-1})[47,48] that spin−orbit effects on the electronic structure are comparable in magnitude to exchange interactions. Thus, a perturbation theory treatment of relativistic or spin−orbit effects is not likely to be sufficient in a system that is as intrinsically relativistic as the bismuth clusters.

In Section II, the experimental methods employed in this investigation are described; the results of our studies are presented in Section III. A discussion of these results and their relationship to previous experimental and theoretical studies is provided in Section IV. Section V then concludes the article with a summary of our findings.

II. Experiment

The optical spectrum of Bi_3 has been investigated using resonant two-photon ionization (R2PI) spectroscopy with time-of-flight mass spectrometric detection. Details of the R2PI apparatus used for this investigation have been described previously.[49] A bismuth molecular beam was created by pulsed laser ablation (Nd:YAG laser, 532 nm, 15 mJ/pulse, 10 Hz repetition rate) of a bismuth target disk. The ablation laser pulse was timed to coincide with the peak density of a helium pulse produced by a double solenoid pulsed nozzle, also operating at 10 Hz and with a backing pressure of 120 psi. A 2 mm diameter, 3 cm long exit channel allowed cluster formation prior to expansion into vacuum, thereby producing a significant concentration of Bi_3 in the molecular beam. Bismuth clusters from the atom to Bi_5 were readily produced and detected under these conditions. Twenty centimeters downstream from the expansion orifice the molecular beam was roughly collimated by a 1 cm diameter skimmer. The collimated beam then entered the extraction region of a Wiley−McLaren time-of-flight mass spectrometer[50] that employed a reflectron geometry[51,52] to improve the mass resolution. In this region the molecular beam was spectroscopically probed using a counterpropagated Nd:YAG-pumped dye laser beam having a line width of 0.8 cm^{-1}. After a time delay of about 20 ns, an excimer laser beam was directed across the collinear molecular and dye laser beams, allowing one-photon ionization of any excited molecular states, provided that the ionization limit is energetically accessible. Ionized species were separated by the time-of-flight mass spectrometer and detected using a microchannel plate detector. By scanning the dye laser frequency and recording the ion signal at a specific mass as a function of wavenumber, the optical spectrum was obtained. In all of the experiments described here, the Bi^+, Bi_2^+, Bi_3^+, and Bi_4^+ mass channels were monitored. There were no spectroscopic transitions detected at the masses of Bi_2^+ or Bi_4^+ in the spectral range scanned, which extended from 9180−16 200 cm^{-1}.

To record an R2PI spectrum, the wavelength of the ionization laser must be appropriately chosen. The ionization wavelength must be unable to ionize the ground state of the molecule in a one-photon process; in that case, a large ion signal is observed regardless of whether the spectroscopy laser excites a transition or not. Likewise, the sum of the photon energies of the spectroscopy laser and the ionization laser must exceed the ionization energy of the molecule; otherwise a third photon is required for ionization, severely reducing the efficiency of the ionization process. These requirements complicated our ability to investigate the Bi_3 spectrum.

For the initial investigations of Bi_3, the excimer laser used for photoionization was the KrF laser (248 nm, 5.00 eV). With this ionization laser, the $\tilde{B}-\tilde{X}_1$ spectrum, previously known from matrix isolation work,[40,41] was readily observed in the 15 000−16 000 cm^{-1} range. The $\tilde{B}-\tilde{X}_1$ spectrum could not be recorded using ArF excimer radiation (193 nm, 6.42 eV) for ionization, presumably because Bi_3 is one-photon ionized at this wavelength. This possibility is supported by the work of Yoo et al., who find $IE(Bi_3) \leq 6.36$ eV.[53] When scanning to the red in hopes of finding the $\tilde{A}-\tilde{X}_1$ band system that was reported in matrix isolation work and assigned to Bi_4 at $T_0 = 12{,}396$ cm^{-1},[40,41] we were unable to observe this state using KrF excimer radiation (248 nm, 5.00 eV) as the ionization wavelength. A possible explanation for our failure to observe the $\tilde{A}-\tilde{X}_1$ band system could be that the combination of the spectroscopy photon energy and the KrF excimer laser energy had dropped below the ionization energy of the molecule, thereby preventing a successful resonant two-photon ionization process from occurring.

To improve our chances for success in locating transitions in the near-infrared region, it became necessary to use an ionization wavelength between 248 nm (KrF excimer radiation) and 193 nm (ArF excimer radiation). An appropriate ionization wavelength was generated by Raman shifting ArF excimer radiation in a high pressure (460 psi) H_2 cell.[54,55] The first Stokes radiation at 210 nm (5.90 eV) was then employed as the ionization photon for studies in the near-infrared region. The Raman shifting technique was also employed to create the near-infrared probe laser radiation. In this case, the output of the laser dyes DCM, LDS 698, LDS 750, and LDS 751 was shifted into the near-infrared using a second Raman shifter, again filled with high pressure H_2. The precisely known H_2 Raman shift of 4155.259 cm^{-1} (which varies slightly with H_2 pressure)[56] allowed the spectra to be accurately calibrated based on the wavenumber of the dye laser fundamental. This, in turn, was calibrated at a few specific wavelengths by inserting an intracavity étalon and pressure scanning the laser, while recording an absorption spectrum of I_2 for comparison to the I_2 atlas of Gerstenkorn and Luc.[57,58] It is believed on the basis of these calibrations that the error in reported band positions for strong, sharp features in the spectrum is below 2 cm^{-1}.

Production of the 5.90 eV (210 nm) ionization radiation employed a high pressure H_2 cell 27 in. long and 1 in. in diameter. The cell was closed with 1 in. thick, 2 in. diameter fused silica windows (Corning 7940-UV) rated for a pressure of 2000 psi with a safety factor of 10. This material allowed transmission of the fundamental ArF (193 nm) and the first Stokes (210 nm) radiation, but absorbed the first anti-Stokes radiation (179 nm). The excimer laser operating on an ArF gas mixture was fitted with unstable resonator optics to provide a highly collimated beam suitable for the tight focusing required for efficient Raman shifting. The ArF laser output (80 −120 mJ/pulse) was focused by a 1 in. diameter UV grade lens (focal length 70 cm at 500 nm) to a spot size approximately 2 mm × 1 mm in the center of the H_2 cell. The Stokes radiation (210 nm) and the residual fundamental radiation were then collimated with a second lens that was identical to the focusing lens. The Stokes radiation was then separated from the fundamental radiation using a dielectric coated mirror that reflected 95% of the 193 nm radiation and transmitted 70% of the 210 nm radiation. The small amount of 193 nm radiation that was transmitted proved to be sufficient to one-photon ionize enough

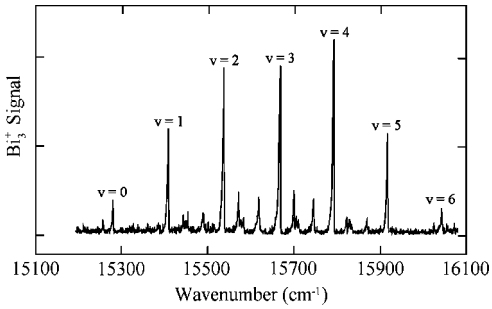

Figure 1. The Bi_3 $\tilde{B} \leftarrow \tilde{X}_1$ band system.

Bi_3 molecules to make a resonance-enhanced spectrum undetectable. This residual 193 nm radiation was removed using a 1 cm thick KBr salt window that transmitted roughly 30% of the 210 nm light. Other salt windows (NaCl and CsI) were also effective in completely absorbing the residual ArF radiation while still passing sufficient quantities of the 210 nm radiation for photoionization. While inconvenient, these techniques permitted the near-infrared spectrum of Bi_3 to be successfully recorded. We estimate that this method provided pulse energies at the 210 nm wavelength of about 5 mJ/pulse.

Excited state lifetime measurements were performed using a time-delayed resonant two-photon ionization technique. By varying the interval between the excitation and ionization laser pulses and measuring the ion signal as a function of this delay, an exponential decay curve was recorded. This waveform was then fitted to extract the excited-state lifetime using the Marquardt nonlinear least-squares algorithm.[59]

III. Results

Through the use of the Raman shifted ArF radiation (210 nm, 5.90 eV) for ionization, the entire spectral region 9180−16 150 cm^{-1} (1089−619 nm) was scanned. In addition, the regions between 15 150 and 16 200 cm^{-1} (660−617 nm), 14 200−14 600 cm^{-1} (705−685 nm), 12 500−13 420 cm^{-1} (800−745 nm), and 10 030−10 440 cm^{-1} (997−958 nm) were also scanned using KrF excimer radiation (248 nm, 5.00 eV) for ionization. No transitions were observed at the masses of Bi_2 or Bi_4. In contrast, two band systems were recorded at the mass of Bi_3.

It has been noted above that the $\tilde{B}-\tilde{X}_1$ system, found in the 15 100−16 100 cm^{-1} range was previously observed in crogenic rare gas matrices and was assigned to Bi_4. In our experiments, these features and the 9 600−10 600 cm^{-1} system both show up at the mass of Bi_3. Furthermore, only small amounts of Bi_4 were evident in the molecular beam. While in principle one should consider the possibility that the transitions are due to Bi_4, and that the electronically excited Bi_4 somehow fragments to form an electronically excited-state of Bi_3, which is then efficiently ionized by the excimer laser, there is no experimental data to support this possibility. If such a process were occurring, one would expect some kinetic energy release during the fragmentation process, leading to a broadening of the Bi_3 peak in the mass spectrum. Alternatively, if fragmentation occurred after ionization, the ions would be accelerated as Bi_4^+ for a portion of the acceleration time and as Bi_3^+ for the remainder of the time, leading to a tailing of the mass peak toward longer flight times (higher masses). In contrast to these predictions, the mass peak on resonance was simply a magnified version of the off-resonant feature with no broadening or tailing toward higher masses evident. On this basis, we are confident that the spectroscopic features reported here are truly due to Bi_3 and not Bi_4.

TABLE 1: The [15.3]$\tilde{B}-\tilde{X}$ System of Bi_3[a]

designation	wavenumber (cm^{-1})	relative intensity	upper state lifetime (ns)
1_1^1	15258.0	6	hot band
0_0^0	15279.4	17	674
1_1^2	15387.1	3	hot band
1_0^1	15407.7	53	308
2_0^2[a]	15445.0	8	
	15451	6	
	15456.1	10	
3_0^3[a]	15489.6	8	
1_1^3	15513.8	3	hot band
1_0^2	15535.3	84	213
$1_0^1 2_0^2$[a]	15571.5	22	
$1_0^1 3_0^3$[a]	15616.6	19	
1_0^3	15662.6	87	124
$1_0^2 2_0^2$[a]	15697.0	22	
	15703.0	10	
	15709.1	7	
$1_0^2 3_0^3$[a]	15742.6	18	
1_0^4	15789.2	100	60
$1_0^3 2_0^2$[a]	15822.3	8	
	15829.5	7	
	15834.3	5	
$1_0^3 3_0^3$[a]	15868.2	8	
1_0^5	15914.7	51	44
1_0^6	16040.7	12	13

[a] Excitations of the bending modes labeled 2_0^2 or 3_0^2 are labeled as they were in the original matrix isolation investigation (ref 41). It is likely that these levels are more properly considered in the context of a $^2E'$ excited-state that is subject to a Jahn−Teller effect.

A. The [15.3] $\tilde{B}-\tilde{X}_1$ System. Figure 1 displays the spectrum of Bi_3 in the 15 100−16 100 cm^{-1} range, as recorded using DCM laser dye and KrF radiation (248 nm, 4.997 eV) for photoionization. The identical spectrum was also recorded using 210 nm radiation for photoionization. The observed vibronic transitions are listed in Table 1. The spectrum is characterized by a weak origin band at 15 279 cm^{-1} and is dominated by an intense series of features forming a vibrational progression that can be fitted to the anharmonic formula[60]

$$v = T_0 + v_1\omega_1 + (v_1^2 + v_1)x_{11} \qquad (3.1)$$

with $T_0 = 15{,}279.4(2)$, $\omega_1 = 128.8(2)$, and $x_{11} = -0.28(2)$ cm^{-1}, where the 1σ error limits are provided in parentheses. The quality of the least-squares fit is excellent with the largest error in the fit being 0.4 cm^{-1}. The mode that is active in this electronic transition is expected to be the totally symmetric breathing mode, assuming that the molecule has a geometry that is close to D_{3h}.

In addition to the strong features, three weak features are found just to the red of the 0_0^0, 1_0^1, and 1_0^2 bands. Anything to the red of the 0_0^0 band must be a vibrational hot band, arising from an excited vibrational level that remains populated in the jet-cooled molecular beam. These weak features lie only 21 cm^{-1} to the red of the 0_0^0, 1_0^1, and 1_0^2 bands, an interval that is too small to be considered as a ground-state vibrational frequency. If the three hot bands are considered to be based on the 1_0^1, 1_0^2, and 1_0^3 bands, then the populated vibrational level in the ground state lies 149 cm^{-1} above the ground vibronic level. This is quite reasonable for a vibrational motion in Bi_3. Furthermore, this value is consistent with the results of matrix isolation resonance Raman[61] and dispersed fluorescence studies,[40,41,43,44] which demonstrate a vibrational progression with $\omega_1'' = 149.7$ cm^{-1} and $x_{11}'' = -0.14$ cm^{-1} in neon

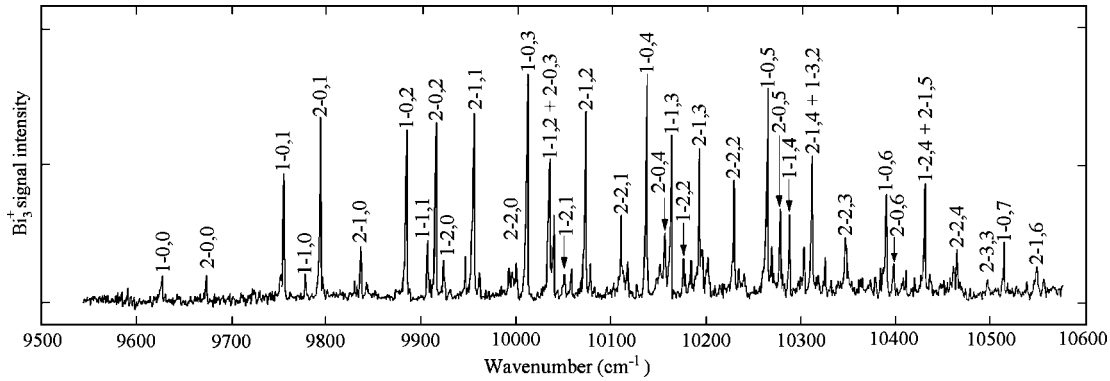

Figure 2. The Bi_3 $\tilde{A}' \leftarrow \tilde{X}_1$ band system. The labeling scheme identifies the $\tilde{A}_1'$ (0, 6) $\leftarrow \tilde{X}_1$ (0) band listed in Table 2, for example, as the 1-0,6 band. This more compact notation permits the use of larger labels in the figure.

matrices.[41] Accordingly, these three bands are identified as the 1_1^1, 1_1^2, and 1_1^3 bands. In the matrix isolation investigations, the carrier of the spectrum was tentatively assumed to be Bi_4; the mass-resolved R2PI spectrum obtained here demonstrates that the carrier is instead Bi_3.

The matrix isolation fluorescence excitation spectrum recorded by Bondybey and English in solid neon shows significantly more features than our gas-phase spectrum, with far greater intensity in the higher members of the vibrational progression, which in their work extends up to $v_1' = 8$.[41] Measurements of single vibronic level lifetimes, performed by time-delayed R2PI techniques, provides an explanation for the difference between the matrix isolation and the R2PI spectra. As shown in Table 1 the measured lifetimes show a strong dependence on the vibrational quantum number, v_1', dropping by about a factor of 2 for each incremental increase in v_1', from 674 ns for $v_1' = 0$ to 13 ns for $v_1' = 6$. Such a rapid variation in excited-state lifetime cannot be due to the dependence of the transition moment on the nuclear positions. Instead, it must be due to predissociation of the electronically excited Bi_3 molecule, which becomes more rapid as the molecule is vibrationally excited within the $\tilde{B}$ electronic state. Above $v_1' = 6$, predissociation apparently occurs too rapidly for the excited molecule to be photoionized in our experiment. Predissociation at the energies probed in the $\tilde{B} \leftarrow \tilde{X}_1$ system is certainly a possibility in this molecule, since the published ΔH_{f0}° values for Bi, Bi_2, and Bi_3 combine to give the bond dissociation energy of $D_0(Bi_2-Bi) = 1.54 \pm 0.05$ eV, or $12\,400 \pm 400$ cm^{-1}.[53] Predissociation is expected to be a much less efficient process in cryogenic rare gas matrices, due to caging effects and rapid deactivation of the molecule to the ground vibronic level of the $\tilde{B}$ state (as observed in neon matrices)[41] or to the lower-lying $\tilde{A}$ electronic state (as observed in argon matrices).[41] A process of rapid vibrational deactivation to the ground level of the $\tilde{B}$ state would then allow higher vibronic levels to be observed by fluorescence action spectroscopy, as was accomplished in the matrix experiments.[41]

Finally, the spectrum also displays additional features between the peaks of the strong vibrational progression that are more difficult to interpret. These were also observed in the matrix isolation studies,[41] where the features are sharper and persist to higher vibrational levels. In that investigation,[41] these features were assigned to two additional antisymmetric normal modes of Bi_4; for Bi_3 the detection of two additional normal modes would exhaust the set of vibrational modes available in the triatomic molecule. In the matrix isolation work, values of (v_2', v_3') of (2, 0), (4, 0), (0, 2), and (2, 2) were assigned, consistent with the requirement that antisymmetric modes are expected to be visible only for even values of Δv. In contrast, in the present gas-phase study only the peaks previously assigned to $(v_2', v_3') = (2, 0)$ and (0, 2) could be detected. It appears that excitation of the higher (v_2', v_3') levels increases the predissociation rate substantially more than placing a similar amount of energy in the v_1' mode, causing many of the levels observed in the matrix isolation experiments to be absent in our spectrum. In Section IV.B.3 we discuss the $\tilde{B}$ state of Bi_3 in greater detail and suggest that although these excitations of the bending mode can be fitted to a harmonic model, this may be an accident. It is perhaps more likely that the $\tilde{B}$ state is a Jahn−Teller active $^2E'$ state for which the bending levels that are accessed from the ground state happen by chance to fit the harmonic model.

B. The [9.6] $\tilde{A}' \leftarrow \tilde{X}_1$ System. In the near-infrared region, a complicated band system comprising over 50 bands is found. This is a new system, which was not observed in the previous matrix isolation investigations. In order to maintain the labeling of the previous work, in which a band system with $T_0 = 12\,396$ cm^{-1} is assigned to the $\tilde{A} \leftarrow \tilde{X}_1$ band system,[41] we designate this new system as the [9.6] $\tilde{A}' \leftarrow \tilde{X}_1$ band system. Here, as in the [15.3] $\tilde{B}$ state, the value reported in square brackets represents the term energy of the vibrationless level of the state, in units of kiloKaysers (1000 cm^{-1}). The [9.6] $\tilde{A}' \leftarrow \tilde{X}_1$ band system is displayed in Figure 2 and band positions are listed in Table 2.. The strong features in the spectrum may be readily grouped into about eight progressions, all characterized by an upper state frequency of about 125 cm^{-1}. A more detailed examination of these progressions shows that they break into two sets. One set has a frequency of about 128 cm^{-1}, while the other has a frequency of about 119 cm^{-1}. Further, when examining the transitions within each set, a second progression is found with a frequency of about 160 cm^{-1}. Thus, it is possible to classify nearly all of the observed bands in this region into two overlapping band systems, with $\omega_1 \approx 160$ cm^{-1} and $\omega_2 \approx 125$ cm^{-1}. The two band systems, which are designated as the $\tilde{A}_1' \leftarrow \tilde{X}_1$ and $\tilde{A}_2' \leftarrow \tilde{X}_1$ systems, may be fitted to the standard anharmonic formula[60]

$$v = T_0 + \omega_1' v_1 + \omega_2' v_2 + x_{11}'(v_1^2 + v_1) + x_{22}'(v_2^2 + v_2) + x_{12}'(v_1 v_2 + v_1/2 + v_2/2) \quad (3.2)$$

where the fitted parameters $\{T_0, \omega_1', \omega_2', x_{11}', x_{22}', \text{and } x_{12}'\}$ are listed in Table 3, along with fitted parameters for the $\tilde{X}_1$ and $\tilde{B}$ states.

Table 3 shows that the $\tilde{A}_1'$ and $\tilde{A}_2'$ states have similar vibrational frequencies, making it tempting to try to identify a

TABLE 2: The [9.6] $\tilde{A}'-\tilde{X}$ System of Bi_3[a]

designation	wavenumber (cm^{-1})	residual (cm^{-1})	relative intensity	upper state lifetime (μs)
$\tilde{A}_1'$ (0, 0) ← $\tilde{X}_1$ (0)	9626.1	−0.2	10	
$\tilde{A}_2'$ (0, 0) ← $\tilde{X}_1$ (0)	9672.2	−0.7	10	
$\tilde{A}_1'$ (0, 1) ← $\tilde{X}_1$ (0)	9755.5	0.3	54	17.1 ($\tilde{A}_1$)
$\tilde{A}_1'$ (1, 0) ← $\tilde{X}_1$ (0)	9778.1	−0.8	10	
$\tilde{A}_2'$ (0, 1) ← $\tilde{X}_1$ (0)	9794.1	0.3	79	32.6 ($\tilde{A}_2$)
$\tilde{A}_2'$ (1, 0) ← $\tilde{X}_1$ (0)	9836.5	1.6	23	
$\tilde{A}_2'$ (2, 0) ← $\tilde{X}_1$ (1)	9842.8		6	hot band
$\tilde{A}_1'$ (0, 2) ← $\tilde{X}_1$ (0)	9884.0	0.5	75	13.8 ($\tilde{A}_1$)
$\tilde{A}_1'$ (1, 1) ← $\tilde{X}_1$ (0)	9906.9	−0.4	25	
$\tilde{A}_2'$ (0, 2) ← $\tilde{X}_1$ (0)	9915.1	0.3	77	35.0 ($\tilde{A}_2$)
$\tilde{A}_1'$ (2, 0) ← $\tilde{X}_1$ (0)	9923.3	0.5	17	
unassigned	9946.5		17	
$\tilde{A}_2'$ (1, 1) ← $\tilde{X}_1$ (0)	9954.8	0.7	79	30.1 ($\tilde{A}_2$)
$\tilde{A}_2'$ (2, 1) ← $\tilde{X}_1$ (1)	9961.2		10	hot band
$\tilde{A}_1'$ (0, 4) ← $\tilde{X}_1$ (1)	9988.6		11	hot band
$\tilde{A}_2'$ (2, 0) ← $\tilde{X}_1$ (0)	9992.5	−2.1	10	
unassigned	10000.4		13	
$\tilde{A}_1'$ (0, 3) ← $\tilde{X}_1$ (0)	10011.3	0.2	100	10.6 ($\tilde{A}_1$)
$\tilde{A}_1'$ (1, 2) ← $\tilde{X}_1$ (0) $\tilde{A}_2'$ (0, 3) ← $\tilde{X}_1$ (0)	10035.1	0.2 −0.6	62	21.9 ($\tilde{A}_1 + \tilde{A}_2$)
$\tilde{A}_2'$ (1, 3) ← $\tilde{X}_1$ (1)	10040.0		35	hot band
$\tilde{A}_1'$ (2, 1) ← $\tilde{X}_1$ (0)	10051.5	1.0	10	
$\tilde{A}_1'$ (3, 0) ← $\tilde{X}_1$ (0)	10058.8	1.0	13	
$\tilde{A}_2'$ (1, 2) ← $\tilde{X}_1$ (0)	10073.1	−0.1	81	24 ($\tilde{A}_2$)
$\tilde{A}_2'$ (2, 2) ← $\tilde{X}_1$ (1)	10078.7		13	hot band
$\tilde{A}_2'$ (2, 1) ← $\tilde{X}_1$ (0)	10111.5	−0.5	37	
$\tilde{A}_2'$ (3, 1) ← $\tilde{X}_1$ (1)	10118.0		15	hot band
$\tilde{A}_1'$ (0, 4) ← $\tilde{X}_1$ (0)	10137.9	−0.2	98	21.9 ($\tilde{A}_1$)
$\tilde{A}_2'$ (3, 0) ← $\tilde{X}_1$ (0)	10152.9	0.8	14	
$\tilde{A}_2'$ (0, 4) ← $\tilde{X}_1$ (0)	10156.7	0.1	29	
$\tilde{A}_1'$ (1, 3) ← $\tilde{X}_1$ (0)	10162.9	1.0	71	11.7 ($\tilde{A}_1$)
$\tilde{A}_1'$ (2, 2) ← $\tilde{X}_1$ (0)	10176.0	−1.5	15	
$\tilde{A}_1'$ (3, 1) ← $\tilde{X}_1$ (0)	10183.5	−1.4	13	
$\tilde{A}_2'$ (1, 3) ← $\tilde{X}_1$ (0)	10192.2	−0.2	65	14.0 ($\tilde{A}_2$)
$\tilde{A}_2'$ (2, 3) ← $\tilde{X}_1$ (1)	10200.7		15	hot band
$\tilde{A}_2'$ (2, 2) ← $\tilde{X}_1$ (0)	10228.7	−0.7	48	
unassigned	10234.1		8	
$\tilde{A}_1'$ (0, 6) ← $\tilde{X}_1$ (1)	10240.2		6	hot band
$\tilde{A}_1'$ (0, 5) ← $\tilde{X}_1$ (0)	10264.0	−0.3	87	5.2 ($\tilde{A}_1$)
$\tilde{A}_2'$ (3, 1) ← $\tilde{X}_1$ (0)	10268.7	0.9	15	
$\tilde{A}_2'$ (0, 5) ← $\tilde{X}_1$ (0)	10277.6	0.1	35	
$\tilde{A}_1'$ (1, 4) ← $\tilde{X}_1$ (0)	10287.9	−0.3	35	
$\tilde{A}_1'$ (2, 3) ← $\tilde{X}_1$ (0)	10303.1	−0.8	19	
$\tilde{A}_1'$ (3, 2) ← $\tilde{X}_1$ (0) $\tilde{A}_2'$ (1, 4) ← $\tilde{X}_1$ (0)	10311.6	0.3 0.1	58	
unassigned	10325.7		13	
$\tilde{A}_2'$ (2, 3) ← $\tilde{X}_1$ (0)	10347.1	0.3	23	
$\tilde{A}_1'$ (0, 6) ← $\tilde{X}_1$ (0)	10389.8	−0.1	44	9.6 ($\tilde{A}_1$)
$\tilde{A}_2'$ (0, 6) ← $\tilde{X}_1$ (0)	10398.1	−0.3	12	
$\tilde{A}_1'$ (2, 4) ← $\tilde{X}_1$ (0) $\tilde{A}_2'$ (1, 5) ← $\tilde{X}_1$ (0)	10430.8	1.2 0.1	44	6.1 ($\tilde{A}_1 + \tilde{A}_2$)
$\tilde{A}_2'$ (2, 4) ← $\tilde{X}_1$ (0)	10465.2	1.0	19	
$\tilde{A}_2'$ (3, 3) ← $\tilde{X}_1$ (0)	10498.1	−1.0	6	
$\tilde{A}_1'$ (0, 7) ← $\tilde{X}_1$ (0)	10514.8	0.0	21	
$\tilde{A}_2'$ (1, 6) ← $\tilde{X}_1$ (0)	10549.8	0.0	10	

[a] The designation for the $\tilde{A}'$ levels only lists two vibrational quantum numbers, corresponding to the values for the ω_1' totally symmetric breathing mode (which is assumed to be the higher frequency mode) and for the ω_2' bending mode, which is of e′ symmetry. All of the assigned transitions originate from either the vibrationless level of the $\tilde{X}_1$ state or from the $v_1'' = 1$ level, corresponding to one excitation of the totally symmetric breathing mode. For this reason, only the value of v_1'' is listed in the assignment, as $\tilde{X}_1$ (v'').

third normal mode, so that the $\tilde{A}_1'$ system corresponds to $v_3' = 0$ while the $\tilde{A}_2'$ system has $v_3' = 1$. Three facts argue against this possibility. First, the apparent origin bands of the two systems, given by T_0 values of 9626 and 9673 cm^{-1}, are separated by only 47 cm^{-1}, a value that seems too small to correspond to a normal mode of Bi_3. Second, given the comparable intensity of the $\tilde{A}_1' \leftarrow \tilde{X}_1$ and $\tilde{A}_2' \leftarrow \tilde{X}_1$ systems, one would expect to observe higher members of a progression in the third normal mode, v_3'. Although a few unexplained bands are present in the spectrum, they are much weaker than would be expected, and are not consistent with values of $v_3' = 2$ or higher. Finally, the excited-state lifetimes measured for the strong bands show significantly longer lifetimes for the $\tilde{A}_2'$ levels, averaging 27 μs, compared to the $\tilde{A}_1'$ levels, which average 13 μs. One would normally expect levels that differ only in the value of v_3' to have similar lifetimes, unless predissociation is occurring. Predissociation is not a possibility at the energy of the $\tilde{A}'$ state.

An alternate possibility is that a low-lying vibrational level of Bi_3 is strongly populated in the molecular beam, so that the $\tilde{A}_1' \leftarrow \tilde{X}_1$ system is simply a red-shifted version of the $\tilde{A}_2' \leftarrow \tilde{X}_1$ system. If this were the case, the upper levels of the two systems would be the same. This is clearly not true, based on the different excited-state lifetimes and the different vibrational constants for the two systems. On the basis of these facts, we are forced to conclude that we are observing two overlapping band systems with similar vibrational frequencies. In Section IV below we argue that these two band systems are likely spin−orbit components of a single excited electronic state.

C. Ionization Energy of Bi_3. The resonant two-photon ionization technique often provides an accurate bracketing of the ionization energy of molecular species.[62,63] In the present study, an absolute upper limit, IE(Bi_3) ≤ 6.89 eV, is established by the observation of the origin band of the [15.3] $\tilde{B}-\tilde{X}_1$ transition at $v_{00} = 15\,279.4$ cm^{-1} with KrF (4.997 eV) ionization radiation. The [15.3] $\tilde{B}-\tilde{X}_1$ band system is not observed when the ArF (6.42 eV) ionizing laser is employed, strongly suggesting that ArF radiation is capable of ionizing Bi_3 by absorption of a single photon. This would imply that IE(Bi_3) < 6.42 eV. The upper limit set by the ArF excimer experiment could be in error due to the outside possibility of a resonance in the neutral molecule at 193 nm, which could cause the two-photon ionization process to be very efficient, and thereby to appear to be a one-photon process. A lower limit for the ionization energy of Bi_3 has also been established using the lower energy band system. Using KrF ionization radiation, none of the bands of the $\tilde{A}' \leftarrow \tilde{X}_1$ band system in the range of 10 030−10 440 could be observed. The fact that the 10 430 cm^{-1} band of this system could not be observed with KrF radiation then implies that IE(Bi_3) > 6.29 eV.

If it is accepted that the absorption of a single ArF photon at 193 nm ionizes the Bi_3 molecule, these observations place the IE(Bi_3) in the range 6.29 eV < IE(Bi_3) < 6.42 eV, or IE(Bi_3) = 6.36 ± 0.07 eV. We believe this result is valid, as it is in excellent agreement with the upper limit determined by Yoo et al. in a photoion yield experiment, which found IE(Bi_3) ≤ 6.36 eV.[53] It is also in good agreement with the value obtained in ab initio multireference configuration interaction calculations, 6.16 eV.[23] Our value of IE(Bi_3) is in disagreement with an earlier investigation, which found Bi_3 to be two-photon ionized at the wavelength of the F_2 excimer laser, placing IE(Bi_3) > 7.89 eV.[64] This value is completely out of the range of possibility based on the present investigation. It is likely that a major contributor to the Bi_3^+ signal in this early experiment resulted from two-photon absorption in a larger Bi_n cluster at 157 nm, leading to efficient ionization and fragmentation to produce a Bi_3^+ fragment. Such a process would lead to a Bi_3^+ signal that depends quadratically on the fluence of the 157 nm radiation and could be interpreted as evidence that IE(Bi_3) > 7.89 eV. Another early report, which provided the estimate IE(Bi_3) = 7.9 ± 0.2 eV by an electron impact investigation,[65] is also far outside of the range of possibility based on the present study.

TABLE 3: Fitted Parameters

parameter	$\tilde{X}_1$ state	$\tilde{A}_1'$ state	$\tilde{A}_2'$ state	$\tilde{B}$ state
T_0 (cm^{-1})		9626.28(67)	9672.93(68)	15 279.43(20)
ω_1 (cm^{-1})	v_1 = 149.5(1.5)	161.80(104)	165.10(99)	128.80(18)
ω_2 (cm^{-1})		129.95(54)	121.80(53)	
x_{11} (cm^{-1})		−4.41(22)	−1.12(21)	−0.279(25)
x_{22} (cm^{-1})		−0.34(6)	−0.002(63)	
x_{12} (cm^{-1})		−0.63(16)	−1.76(13)	
number of measured bands	11	21	22	7
rms error (cm^{-1})	1.40	0.73	0.77	0.17
maximum absolute error (cm^{-1})	3.14	1.54	2.14	0.37

IV. Discussion

A. Electronic Structure of Bi_3. Atomic bismuth has a ground-state valence electron configuration of $6s^2\ 6p^3$, ^4S_u. Removal of a 6p electron to form Bi^+ in its $6s^2\ 6p$, $^2\ ^3P_0$ ground state requires 7.286 eV,[66] while removal of a 6s electron to form Bi^+ in its $6s^1\ 6p^3$, ^5S_u state requires 16.726 eV.[67] This large difference in ionization energies demonstrates the relativistic stabilization of the 6*s* orbital, which causes the 6s electrons in bismuth to be unimportant for a zeroth-order description of the chemical bonding. By counting these electrons as members of the valence space and including all of the valence electrons in the numbering of the molecular orbitals, the 6s atomic orbitals combine to form the $1a_1'$ and $1e'$ orbitals in the Bi_3 molecule in the equilateral, D_{3h}, geometry. These orbitals are undoubtedly fully occupied in all of the electronic states of Bi_3 that have been spectroscopically investigated. Indeed, excitations out of the $1a_1'$ or 1e orbitals of Bi_3 may even lie above the ionization limit of the molecule.

The real issue in the orbital structure of Bi_3 concerns the 6p orbitals. This set of nine atomic basis functions provides a reducible basis set that decomposes to $A_1' \oplus A_2' \oplus 2E' \oplus A''_2 \oplus E''$ in the D_{3h} point group. To understand the molecular orbitals of this system in greater detail, it is useful to subdivide the set of nine atomic 6p orbitals into the three radially directed 6p orbitals, which point out from the center of the equilateral triangle and lead to molecular orbitals of $A_1' \oplus E'$ symmetry; the three tangentially oriented 6p orbitals, which lie in the plane of the molecule but are orthogonal to the radially directed orbitals and which lead to molecular orbitals of $A_2' \oplus E'$ symmetry; and the three 6pπ orbitals that are oriented out of the plane of the molecule, which lead to molecular orbitals of $A_2'' \oplus E''$ symmetry. Depictions of these molecular orbitals are provided in Figure 3, assuming no mixing between the orbitals of E′ symmetry deriving from the radially directed and tangentially oriented 6p orbitals.

In addition to depicting the linear combinations of the atomic orbitals, Figure 3 also provides the orbital energies in the Hückel approximation, where the interaction between orbitals on adjacent bismuth atoms are given by β_π if the orbitals are perpendicular to the line connecting the atoms, by β_T if the orbitals are oriented at 60° relative to the line connecting the atoms (as is the case for the tangentially oriented 6p orbitals), and by β_R if the orbitals are oriented at 30° relative to the line connecting the atoms, as in the radially directed 6p orbitals. Remembering that all β values are negative, indicating a stabilizing interaction, it is obvious that $\beta_R < \beta_T < \beta_\pi$, since the overlap between orbitals worsens in this series. The definitions of β_R, β_T, and β_π are shown in Figure 4.

With these facts in mind, it is straightforward to rank-order the orbitals deriving from the 6p atomic orbitals as $2a_1' < (1a_2'', 2e') < 1e'' < (3e', 1a_2')$. The ambiguity in the relative energies of the $1a_2$" and 2e′ orbitals derives from the fact that although $\beta_T < \beta_\pi$, it is not so obvious how $2\beta_\pi$ compares to β_T. Likewise, there is a similar ambiguity in the ordering of the 3e′ and $1a_2'$ orbitals. Although $-\beta_T < -\beta_R$, it is again not obvious how $-\beta_R$ compares to $-2\beta_T$. Ab initio calculations suggest that the ordering of the $1a_2''$ and 2e′ orbitals is $1a_2'' < 2e'$,[22,23] although these orbitals are probably not very different in energy, in part due to a lowering of the 2e′ orbital that is expected due to mixing with the 3e′ orbital.

The six 6s electrons and the nine 6p electrons of Bi_3 fill the molecular orbitals to form a ground electronic configuration of $1a_1'^2\ 1e'^4\ 2a_1'^2\ 1a_2''^2\ 2e'^4\ 1e''^1$, giving the ground $^2E''$ term that both theoretical studies find to be the ground state.[22,23] This state is subject to both the Jahn−Teller effect (due to the orbital degeneracy) and to spin−orbit splitting (arising from the

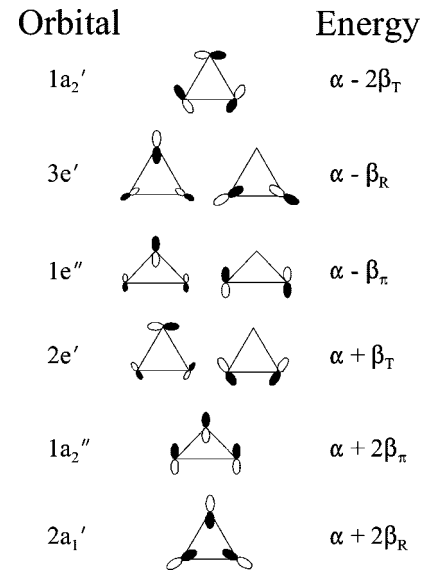

Figure 3. Hückel molecular orbitals formed from the 6p orbitals on the three bismuth atoms. Orbital labels and Hückel energies are provided. See text for details.

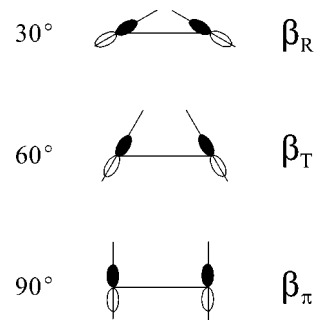

Figure 4. Definition of the β_R, β_T, and β_π resonance integrals. These differ by the angle made between the 6p orbitals and the line connecting the two atomic centers.

TABLE 4: Low-Lying Electronic Configurations and Terms of Bi_3

excitation	configuration	terms
None	$1a_1'^2\ 1e'^4\ 2a_1'^2\ 1a_2''^2\ 2e'^4\ 1e''^1$	$\tilde{X}\ ^2E'$
$1e'' \leftarrow 2e'$	$1a_1'^2\ 1e'^4\ 2a_1'^2\ 1a_2''^2\ 2e'^3\ 1e''^2$	$^2A_1'$, $^2A_2'$, $^2E'(3)$, $^4E'$
$1e'' \leftarrow 1a_2''$	$1a_1'^2\ 1e'^4\ 2a_1'^2\ 1a_2''^1\ 2e'^4\ 1e''^2$	$^2A_1''$, $^2A_2''$, $^2E''$, $^4A_1''$
$3e' \leftarrow 1e''$	$1a_1'^2\ 1e'^4\ 2a_1'^2\ 1a_2''^2\ 2e'^4\ 3e'^1$	$^2E'$
$1a_2' \leftarrow 1e''$	$1a_1'^2\ 1e'^4\ 2a_1'^2\ 1a_2''^2\ 2e'^4\ 1a_2'^1$	$^2A_2'$
$3e' \leftarrow 2e'$	$1a_1'^2\ 1e'^4\ 2a_1'^2\ 1a_2''^2\ 2e'^3\ 1e''^1\ 3e'^1$	$^2A_1''(2)$, $^2A_2''(2)$, $^2E''(6)$, $^4A_1''$, $^4A_2''$, $^4E''(3)$
$3e' \leftarrow 1a_2''$	$1a_1'^2\ 1e'^4\ 2a_1'^2\ 1a_2''^1\ 2e'^4\ 1e''^1\ 3e'^1$	$^2A_1'(2)$, $^2A_2'(2)$, $^2E'(2)$, $^4A_1'$, $^4A_2'$, $^4E'$

TABLE 5: Observed Electronic States of Bi_3

state	T_0 (cm^{-1})	ω_1 (cm^{-1})	ω_2 (cm^{-1})	method
$\tilde{X}_1$	0	149.7 [41]		matrix isolation (Ne, Ar): $\tilde{A} \rightarrow \tilde{X}_1$[40,41] $\tilde{B} \rightarrow \tilde{X}_1$[41] $\tilde{C} \rightarrow \tilde{X}_1$[44] resonance raman [42,44,61]
$\tilde{X}_2$	2170[29]			PES[28,29]
	8500[29]			PES[28,29]
$\tilde{A}_1'$	9626.28(67)	161.80(104)	129.95(54)	PES;[28,29] this work
$\tilde{A}_2'$	9672.93(68)	165.10(99)	121.80(53)	PES;[28,29] this work
$\tilde{A}$	12 396 (Ar)[41] 12 535 (Ne)[42]	~123 (Ar)[40]		PES;[28,29] matrix isolation (Ne, Ar): $\tilde{A} \leftarrow \tilde{X}_1$[40−42] $\tilde{A} \rightarrow \tilde{X}_1$[40,41] not observed in this study
$\tilde{C}$	13 424 (Ne)[44]			PES;[28] matrix isolation (Ne): $\tilde{C} \rightarrow \tilde{X}_1$[44] not observed in this study
$\tilde{B}$	15 279.43(20)	128.80(18)		matrix isolation (Ne, Ar): $\tilde{B} \rightarrow \tilde{X}_1$[41] $\tilde{B} \leftarrow \tilde{X}_1$ [40,41] this work

presence of orbital degeneracy and S = 1/2). The spin−orbit splitting is expected to be significant, because of the huge spin−orbit parameter for the 6p orbital in atomic bismuth, given by $\zeta_{6p}(Bi) \approx 10\ 100\ cm^{-1}$.[68]

The lowest energy excitations in this molecule are likely to be promotion of a 2e′ electron to the 1e″ pair of orbitals, leading to a $1a_1'^2\ 1e'^4\ 2a_1'^2\ 1a_2''^2\ 2e'^3\ 1e''^2$ configuration that generates states of symmetry $^2A_1'$, $^2A_2'$, $^2E'(3)$, and $^4E'$, and promotion of a $1a_2''$ electron to the 1e″ pair of orbitals, leading to a $1a_1'^2\ 1e'^4\ 2a_1'^2\ 1a_2''^1\ 2e'^4\ 1e''^2$ configuration that generates states of symmetry $^2A_1''$, $^2A_2''$, $^2E''$, and $^4A_1''$. Of these, the quartets $^4E'$ and $^4A_1''$ are certainly expected to lie lowest in energy, due to the favorable exchange interactions. The two serious ab initio studies of this molecule that have been undertaken are in general agreement about the location of these quartet states, placing the $^4A_1''$ state in the range of 7000−9200 cm^{-1} above the ground state and the $^4E'$ state in the range of 11 000−13 000 cm^{-1} above the ground state.[22,23] However, there seems to be a confusion in both published papers, in which the $^4A_1''$ state is sometimes mislabeled as a $^4A_2''$ state.[22,23] This makes little sense, because the lowest energy excitation that generates a $^4A_2''$ state is promotion of a 2e′ electron to the 3e′ orbital, which is expected to lie much higher in energy than the $1a_2''$ to 1e″ excitation that leads to the $^4A_1''$ state. Apart from the $^4A_1''$ and $^4E'$ states mentioned above, the only other state that has been reported in computational studies thus far is a $^2E'$ state calculated to lie at about 15 900 cm^{-1}.[23] This state is one of the three $^2E'$ states deriving from the $1a_1'^2\ 1e'^4\ 2a_1'^2\ 1a_2''^2\ 2e'^3\ 1e''^2$ configuration. Given that $^2E'$ states are accessible from the $\tilde{X}^2E''$ ground state by parallel transitions and $^2A_1''$, $^2A_2''$, and $^2E''$ states are accessible by perpendicular transitions, six allowed electronic band systems are expected from the $1e'' \leftarrow 2e'$ and $1e'' \leftarrow 1a_2''$ excitations alone. When the considerable spin−orbit splitting that is expected in this molecule is considered, the number of possible electronic transitions that might be observed becomes very large.

Table 4 presents a list of the expected low-lying configurations in Bi_3, along with the terms deriving from them. It should be remembered that when spin−orbit interactions are considered, all ^2E and ^4A terms split into two doubly degenerate levels and all ^4E terms split into four doubly degenerate levels.[60] The ^2A terms remain doubly degenerate even in the presence of spin−orbit interaction.

B. Experimental Information about the Electronic States of Bi_3. Experimental information about the electronic states of Bi_3 comes from matrix isolation studies,[40,41,43,44,61] photoelectron spectroscopy,[28,29] and the present optical investigation. The overall picture that emerges from these diverse studies is confusing, and would be greatly assisted by detailed theoretical calculations that include a high level of electron correlation and relativistic effects, including spin−orbit interaction. In addition, examination of possible Jahn−Teller distortions would be very helpful in sorting out the details of this molecule. In this section we review the various sources of information to provide an overall picture of the electronic states of triatomic bismuth, up to an energy of 16 000 cm^{-1}. The experimentally observed electronic states of the molecule are summarized in Table 5.

1. The $\tilde{X}^2E''$ Ground State of Bi_3. The qualitative molecular orbital theory described above and ab initio calculations are in absolute agreement that the ground term of Bi_3 arises from the $1a_1'^2\ 1e'^4\ 2a_1'^2\ 1a_2''^2\ 2e'^4\ 1e''^1$ configuration, giving a $^2E''$ ground term.[22,23] Here the unpaired electron occupies an orbital that is composed of 6pπ orbitals directed out of the plane of the molecule, with a single nodal plane perpendicular to the molecular plane, as shown in Figure 3. As such, this is an antibonding orbital. Removal of the 1e″ electron to form the

Bi_3^+ ion then leaves the molecular ion in a closed shell $^1A_1'$ state that is expected to be rigorously D_{3h} in geometry and more strongly bound than the neutral Bi_3 molecule.

Complicating the picture for the Bi_3 ground state is the fact that the $^2E''$ ground state is susceptible to both Jahn−Teller distortion and spin−orbit splitting. Ignoring the spin−orbit effects, the energy difference between the $^2A_2$ (obtuse, $\theta \approx 65°$) and the $^2B_1$ (acute, $\theta \approx 56°$) forms is calculated to be below 0.06 eV (480 cm^{-1}), although which form is more stable varies with the calculational method.[22,23] Limited attempts to include the effects of spin−orbit interaction have been made using relativistic configuration interaction (RCI) methods.[23] Unlike the $\tilde{X}$ ^2E ground states of CH_3O and CH_3S, for example, where the presence of an unpaired electron in an orbital of *e* symmetry on an axial atom causes a first-order spin−orbit splitting, the method of Ichiguro and Kobori shows that there is no first-order spin−orbit splitting in the $\tilde{X}$ $^2E''$ ground state of Bi_3.[69] Instead, spin−orbit splitting in the $\tilde{X}^2E''$ ground state arises in second order via coupling to excited electronic states. This results in a splitting of the $\tilde{X}^2E''$ state that is predicted to be approximately 0.3 eV (2400 cm^{-1}),[23] a value that is much smaller than the spin−orbit parameter of atomic bismuth, given by $\zeta_{6p}(Bi) = 10\,100$ cm^{-1} (1.25 eV).[68]

Spin−orbit splitting in the $\tilde{X}^2E''$ ground state of Bi_3 leads to $E_{1/2}$ and $E_{3/2}$ states in the D_{3h}^2 double group.[60] Because this splitting arises due to interactions with other electronic states, it is impossible to predict which level will emerge as the ground level unless the excited states are carefully treated and a detailed analysis of the off-diagonal spin−orbit interactions is performed. The RCI calculations published to date do not indicate whether the ground level will be of $E_{1/2}$ or $E_{3/2}$ symmetry,[23] but the expected magnitude of the splitting (0.3 eV) is probably an order of magnitude greater than the Jahn−Teller splitting, leading to significant quenching of the Jahn−Teller effect.[23] To distinguish between the two spin−orbit components of the ground $^2E''$ state, we adopt the labels $\tilde{X}_1$ and $\tilde{X}_2$ for the lower and upper components, respectively. Photoelectron spectra of the mass-selected Bi_3^- anion show that the first excited-state of Bi_3 lies about 0.27 eV (2180 cm^{-1}) above the ground state.[29] This is in good agreement with the estimated spin−orbit splitting.[23] We concur with previous investigators[29] that the 2180 cm^{-1} state is the upper spin−orbit component of the $^2E''$ ground state. It is therefore labeled as the $\tilde{X}_2$ $^2E''$ state.

Most of the available information about the $\tilde{X}_1$ ground-state comes from matrix isolation spectroscopy, as the available photoelectron spectroscopic studies lack vibrational resolution.[28,29] The most detailed vibronic information about the $\tilde{X}_1$ ground state comes from the dispersed fluorescence of the $\tilde{B} \rightarrow \tilde{X}_1$ system in solid neon, which established the vibrational constants of the totally symmetric stretching mode as $\omega_1'' = 149.7$ cm^{-1} and $x_{11}'' = -0.14$ cm^{-1}.[41] In that work, additional vibronic levels were detected 180 and 242−245 cm^{-1} above the $v_1'' = 0$ - 2 levels and above the $v_1'' = 0$−6 levels, respectively.[41] These vibronic energy levels can be assigned to Bi_3 with high confidence, since they are part of the $\tilde{B} \leftrightarrow \tilde{X}$ band system that is observed in the present mass-analyzed study.

The $\tilde{X}^2E''$ ground state of Bi_3 is subject to both spin−orbit splitting and the Jahn−Teller effect. A superb review of these effects with emphasis on C_{3v} systems has been provided by Barckholtz and Miller.[70] Likewise, the recent work on Ag_3 published by the Miller group has provided a useful generalization of these results to the case of a D_{3h} triatomic.[71,72] Unfortunately, the knowledge of only two vibronic levels associated with excitations of the Jahn−Teller active e′ mode provides insufficient data for a detailed analysis. A very useful step for the further analysis of this system would be the calculation of an accurate ab initio potential energy surface, including points near the D_{3h} geometry and near the global minimum and saddle point. These could then be used to extract the frequency of the e′ mode, $\omega_{e'}$, as well as the linear and quadratic Jahn−Teller coupling constants, D and K, as was done in the recent investigation of Ag_3.[71] Such an ab initio investigation is well beyond the scope of the present study, however. To provide experimental confirmation of the parameters resulting from such an *ab initio* investigation, it would be necessary to locate additional bending levels in the $\tilde{X}_1$ ground state. Dispersed fluorescence or stimulated emission pumping studies in the gas phase may be able to provide such data.

2. The [9.6] $\tilde{A}'$ $^4A_1''$ State of Bi_3. The next highest energy state of Bi_3 that is vibronically well characterized is the [9.6]$\tilde{A}'$ state, which has first been observed in the present investigation. This state consists of two overlapping electronic substates with vibronic levels that are well described in the harmonic approximation, although small anharmonicities are required to accurately reproduce the levels. The fact that the levels are well described in the harmonic approximation rules out a significant Jahn−Teller effect in this state. On this basis, the state cannot be orbitally degenerate in the D_{3h} point group, a fact that restricts its term symbol to the A_1', A_2', A_1'', or A_2'' irreducible representations. The doublet states, $^2A_1'$, $^2A_2'$, $^2A_1''$, and $^2A_2''$ may also be excluded from consideration, because the Kramers degeneracy cannot be split in the absence of a magnetic field, so there is no way to account for the existence of two overlapping substates. Therefore, we are forced to consider the possibility of the quartet states, $^4A_1'$, $^4A_2'$, $^4A_1''$, and $^4A_2''$. Ab initio calculations predict the lowest quartet state in the molecule to be the $^4A_1''$ state, arising from the $1a_1'^2\ 1e'^4\ 2a_1'^2\ 1a_2''^1\ 2e'^4\ 1e''^2$ configuration, lying in the range of 7000−9200 cm^{-1}.[22,23] This is in reasonably good agreement with the observed location of the [9.6] $\tilde{A}'$ state. Further, the long fluorescence lifetime of the [9.6] $\tilde{A}'$ state (10−30 μs) is consistent with a spin-forbidden [9.6] $\tilde{A}'$ $^4A_1'' \leftrightarrow \tilde{X}_{1,2}$ $^2E''$ transition in a heavy atomic system. Finally, the calculated frequencies[22] of the a_1' breathing mode (144 cm^{-1}) and the e′ bending mode (105 cm^{-1}) in the $^4A_1''$ state are in about the correct ratio and are about 17% too low compared to the measured values (161.80 and 129.95 cm^{-1} for the $\tilde{A}_1'$ substate; 165.10 and 121.80 cm^{-1} for the $\tilde{A}_2'$ substate).

While it is quite common to observe a long progression in a totally symmetric breathing mode in an electronic band system, a long progression in an e′-type bending mode is rare. Ordinarily, nontotally symmetric modes are only observed in multiples of two quanta, and even then a large change in vibrational frequency is required for significant Franck−Condon intensity. Exceptions to this general rule arise when one of the electronic states is Jahn−Teller active. Simulated spectra displayed in Figure 14 of ref 70 show that a transition between the ground level of a Jahn−Teller distorted ^2E state and an undistorted ^2A state can lead to a lengthy progression in the bending mode of the ^2A state. An exactly analogous effect is expected in the case of a $^4A_1'' \leftarrow {}^2E''$ transition that is induced by spin−orbit mixing.

The observation of both the $\tilde{A}_1'$ and $\tilde{A}_2'$ substates with comparable intensities in transitions from the $\tilde{X}_1$ substate carries an implication about the symmetry of the $\tilde{X}_1$ substate. The similar intensities of the $\tilde{A}_1' \leftarrow \tilde{X}_1$ and $\tilde{A}_2' \leftarrow \tilde{X}_1$ subsystems strongly suggest that these transitions are induced by the same component of the electric dipole operator. A detailed examination of the symmetry of the spin−orbit substates in the D_{3h}^2 double group shows that this is only possible if the $\tilde{X}_1$ substate

is the $E_{1/2}$ component of the $\tilde{X}^2E''$ state. To demonstrate this fact, we note that the $\tilde{A}'\ ^4A_1''$ state resolves into $E_{3/2}$ and $E_{5/2}$ substates when spin−orbit interaction is considered.[60] Similarly, the $\tilde{X}^2E''$ state resolves into $E_{1/2}$ and $E_{3/2}$ substates. The electric dipole operator is of symmetry A_2'' (for μ_z, which leads to parallel transitions) and E' (for (μ_x, μ_y), which lead to perpendicular transitions). An examination of the transition dipole integral using the methods of group theory shows that perpendicular transitions are allowed from the $E_{1/2}$ component of the $\tilde{X}^2E''$ ground state to either the $E_{3/2}$ or $E_{5/2}$ component of the $\tilde{A}'\ ^4A_1''$ state, but that the analogous parallel transitions are forbidden. In contrast, transitions from $\tilde{X}\ ^2E''$ ($E_{3/2}$ component) to $\tilde{A}'\ ^4A_1''$ ($E_{3/2}$ component) are allowed for parallel transitions, but forbidden for perpendicular transitions. Exactly the reverse is true for transitions from $\tilde{X}\ ^2E''$ ($E_{3/2}$ component) to $\tilde{A}'\ ^4A_1''$ ($E_{5/2}$ component). These are allowed as perpendicular transitions but forbidden as parallel transitions. Therefore, if we assume that both the $\tilde{A}_1' \leftarrow \tilde{X}_1$ and $\tilde{A}_2' \leftarrow \tilde{X}_1$ subsystems gain their intensity from the same mechanism, the $\tilde{X}_1$ substate must be the $\tilde{X}^2\ E''$, $E_{1/2}$ component.

3. The [15.3]$\tilde{B}$ State of Bi_3. Lying to higher energy is the [15.3]$\tilde{B}$ state, which has been vibronically well characterized by the neon matrix isolation experiments of Bondybey and English,[41] and which has been observed in the gas phase in the present investigation. In addition to a long progression in the totally symmetric breathing mode, the neon matrix isolation experiment reveals four vibronic levels involving excitations of the e′ bending mode that lie 153−164, 202−210, 308−321, and 360−370 cm^{-1} above the corresponding pure breathing mode excitation. Here, the ranges cited for each level reflect a dependence on the number of breathing quanta that are excited. The first two of these excited bending levels have been observed in the present study, but the higher energy bending levels apparently predissociate too rapidly to allow their observation in the gas phase.

As discussed in Section IV.A, the low lying $1e'' \leftarrow 2e'$ and $1e'' \leftarrow 1a_2''$ electronic excitations in Bi_3 lead to $^2A_1'$, $^2A_2'$, $^2E'(3)$, and $^4E'$, and $^2A_1''$, $^2A_2''$, $^2E''$, and $^4A_1''$ terms, respectively. The bending vibronic levels observed by Bondybey and English that are listed above fail to follow the single harmonic progression that would be expected in a transition from a Jahn−Teller active $\tilde{X}^2\ E''$ ($E_{1/2}$ or $E_{3/2}$ component) to an undistorted ^2A state, as is observed in the $\tilde{A}_1'$ and $\tilde{A}_2'$ substates. Instead, they can be fitted to a model in which the degeneracy of the e′ bending mode is split, leading to harmonic progressions in two different modes. This could be an indication that the $\tilde{B}$ state is one of the orbitally nondegenerate ($^2A_1'$, $^2A_2'$, $^2A_1''$, or $^2A_2''$) states that is distorted to a C_{2v} structure, thereby splitting the degeneracy of the e′ mode. Alternatively, the observed vibronic structure could be consistent with a Jahn−Teller active $\tilde{B}\ ^2E$ state, in which the observed vibronic levels happen to fall close to harmonic values. The fact that three $^2E'$ states derive from the $1e'' \leftarrow 2e'$ excitation, and that one of these $^2E'$ states has been calculated to lie at 15 900 cm^{-1},[23] suggests that the observed $\tilde{B}$ state may be one of the spin−orbit components of a Jahn−Teller distorted $^2E'$ state.

4. The [12.4] $\tilde{A}$ State of Bi_3. In matrix isolation work, the [12.4] $\tilde{A} \leftarrow \tilde{X}_1$ absorption system has been observed in cryogenic neon and argon matrices that contain bismuth.[40,42] The [12.4] $\tilde{A} \rightarrow \tilde{X}_1$ emission has also been observed in Ar and Kr matrices, following excitation at either 21 839 cm^{-1} (457.9 nm Ar^+ laser line) or in the [15.3] $\tilde{B} \leftarrow \tilde{X}_1$ system.[40,41] In matrix isolation work, it can be difficult to identify the carrier of a transition with certainty. In this case, however, the band system certainly arises from Bi_3 because the emission system displays a long progression in the totally symmetric breathing mode, which has the same frequency as found in the $\tilde{B} \rightarrow \tilde{X}_1$ dispersed fluorescence.[41] The observation of $\tilde{A} \rightarrow \tilde{X}_1$ emission following excitation of the [15.3] $\tilde{B} \leftarrow \tilde{X}_1$ system also strongly suggests that the carrier is Bi_3. The [12.4] $\tilde{A} \rightarrow \tilde{X}_1$ emission system displays an origin band located at 12 396 cm^{-1} in solid argon, 12 535 cm^{-1} in solid neon.[41,42] In absorption, the system consists of a long progression in a single mode (presumably the totally symmetric breathing mode) with a frequency of 123 cm^{-1}.[40] The system extends from the origin band past 13 222 cm^{-1}.

Our efforts to investigate the spectra of Bi_3 in the near-infrared region were initiated in an attempt to observe the [12.4] $\tilde{A} \leftarrow \tilde{X}_1$ system in the gas phase. Despite careful scans across the 12 500−13 400 cm^{-1} region using KrF excimer radiation for photoionization, we were unsuccessful in observing the system. Fearing that the KrF radiation (248 nm, 5.00 eV) might be insufficient to ionize the molecule from the $\tilde{A}$ state, scans were repeated over the entire 9 180−16 150 cm^{-1} range using Raman-shifted ArF radiation (5.90 eV) for photoionization. Under these conditions, the new [9.6] $\tilde{A}' \leftarrow \tilde{X}_1$ system was found, but the [12.4] $\tilde{A} \leftarrow \tilde{X}_1$ system was again absent. The observation of a band system farther to the red implies that our failure to observe the [12.4] $\tilde{A} \leftarrow \tilde{X}_1$ system could not result from a lack of sufficient energy to ionize the molecule. Further, the observation of the $\tilde{A} \leftarrow \tilde{X}_1$ system in absorption in cryogenic argon matrices shows that the system is an allowed transition. Given these facts, it is surprising that the $\tilde{A} \leftarrow \tilde{X}_1$ system cannot be observed under our experimental conditions. A possible explanation comes from the fact that the published ΔH_{f0}° values for Bi, Bi_2, and Bi_3 combine to give $D_0(Bi_2-Bi) = 1.54 \pm 0.05$ eV, or 12 400 ± 400 cm^{-1}.[53] This value places the $\tilde{A}$ state (T_0 = 12 535 cm^{-1} in solid neon) near or slightly above the dissociation limit. Perhaps the $\tilde{A}$ state undergoes rapid predissociation, so that any Bi_3 molecules excited in this transition are dissociated and cannot contribute to a signal at the mass of Bi_3. As in the case of the $\tilde{B}$ state, rapid predissociation would not prevent the observation of an absorption spectrum. In addition, predissociation would likely be quenched in the argon matrix due to caging effects, allowing the $\tilde{A} \rightarrow \tilde{X}_1$ emission to be observed.

It is not very fruitful to speculate about the symmetry of the $\tilde{A}$ state of Bi_3, since so little is known about it. The frequency of the breathing mode (123 cm^{-1}) is similar to that of the $\tilde{B}$ state (128.8 cm^{-1}), so it is conceivable that the $\tilde{A}$ and $\tilde{B}$ states could be spin−orbit components of the same $^2E'$ state. Confirmation or rejection of this possibility will require state-of-the-art ab initio calculations.

5. Additional Low-Lying States Observed. The $\tilde{X}_1$, $\tilde{X}_2$, and ($\tilde{A}_1'$, $\tilde{A}_2'$) pair of states have been observed in photoelectron spectroscopy of mass-selected Bi_3^- at energies of 0, 2170, and 9710 cm^{-1}, respectively.[29] In a less well-resolved study that extended to higher energies, these levels were observed at 0, 2020, and 10 080 cm^{-1}, respectively.[28] The [12.4] $\tilde{A}$ state is observed as an exceptionally broad and ill-defined feature in the study of Polak et al. and is found in moderate intensity in the study of Gausa et al. near 12 250 cm^{-1}.[28] These results, based on the mass-selected Bi_3^- anion, confirm that these band systems do correspond to transitions in Bi_3, as opposed to a different cluster size.

Both photoelectron investigations show a feature lying below the $\tilde{A}'$ pair of states, but above the $\tilde{X}_2$ state. This strong feature is found at 8500 cm^{-1} in the study by Polak et al. and at 8950 cm^{-1} in the study by Gausa et al.[28,29] Unfortunately, we were unable to investigate states lying this low in energy in our R2PI

study, so we are unable to add any new information about this state. Given that both theoretical investigations predict that the lowest lying excited-state is the $^4A_1''$ state that we have suggested as the upper state in the $\tilde{A}' \leftarrow \tilde{X}_1$ system, it is surprising that another state could exist in this energy range. Choi et al. have calculated that the ground state of Bi_3^- is the $^3A_2'$ state that derives from the $1a_1'^2\ 1e'^4\ 2a_1'^2\ 1a_2''^2\ 2e'^4\ 1e''^2$ configuration, but that a $^1A_1$ (C_{2v}) state lies only about 0.48 eV higher in energy. It is possible that this state is populated in the photoelectron experiments and some of the observed features arise from detachment from it. In the absence of further experimental data and particularly computational work, any further comments about the 8500 cm^{-1} state would be speculative at best.

Finally, the photoelectron experiments of Gausa et al. find a moderately weak feature lying about 13 700 cm^{-1} above the ground state of Bi_3.[28] We find no evidence of this state in our R2PI experiments, but this may again be due to rapid predissociation. Interestingly, Eberle et al. have found evidence of a state in this vicinity in bismuth samples isolated in cryogenic Ne matrices.[44] Eberle and co-workers find that when the Bi_3 excited in the $\tilde{B} \leftarrow \tilde{X}_1$ system in solid neon, a new emission system appears in addition to the known $\tilde{B} \rightarrow \tilde{X}_1$ system. The new emission system, identified as the $\tilde{C} \rightarrow \tilde{X}_1$ system shows a long progression in the totally symmetric breathing mode with the same vibrational frequency as found for the $\tilde{B} \rightarrow \tilde{X}_1$ emission. The new system is about a factor of 10 000 weaker than the $\tilde{B} \rightarrow \tilde{X}_1$ emission and appears to have its origin band near 13 424 cm^{-1}. Regrettably, the system could not be examined in excitation due to an inability to generate laser wavenumbers below 14 400 cm^{-1}. This state could probably be usefully examined by laser excitation spectroscopy of matrix isolated Bi_3, although a careful ab initio treatment will certainly be required to identify the electronic symmetry.

V. Conclusion

Through the use of mass-analyzed resonant two-photon ionization spectroscopy, the previously known $\tilde{A} \leftrightarrow \tilde{X}_1$, $\tilde{B} \leftrightarrow \tilde{X}_1$, and $\tilde{C} \rightarrow \tilde{X}_1$ band systems, which had been assigned via matrix isolation spectroscopy to Bi_4, have now been reassigned to Bi_3. This is consistent with electronic states observed in the photoelectron spectra of mass-selected Bi_3^-. The R2PI spectrum of the $\tilde{B} \leftarrow \tilde{X}_1$ system is nearly identical with that reported in matrix isolation studies, but lifetime measurements show that predissociation occurs in the higher vibrational levels.

In addition, R2PI spectroscopy has revealed a new band system in the 9600−10 600 cm^{-1} range that consists of two overlapping band systems, each with two progression-forming normal modes. The modes of the overlapping band systems are so similar in frequency that it seems likely that the two systems represent different spin−orbit levels of the same electronic term, which is argued to be the $^4A_1''$ term that derives from the $1a_1'^2\ 1e'^4\ 2a_1'^2\ 1a_2''^1\ 2e'^4\ 1e''^2$ electronic configuration. The ground state may be considered to be well established as having $^2E''$ electronic symmetry, deriving from the $1a_1'^2\ 1e'^4\ 2a_1'^2\ 1a_2''^2\ 2e'^4\ 1e''^1$ electronic configuration. Spin−orbit splitting causes this state to split into $E_{1/2}$ and $E_{3/2}$ levels, resulting in the partial quenching of the Jahn−Teller effect. The observation of both components of the $^4A_1''$ term in comparable intensity suggests that the ground level is the $E_{1/2}$ component.

A review of the experimentally known electronic states of Bi_3 shows that there are at least eight substates lying below 16 000 cm^{-1}. To completely sort these out will require high-level ab initio calculations that incorporate relativistic and spin−orbit effects. In this regard, Bi_3 represents a severe challenge to ab initio quantum chemistry.

Acknowledgment. This material is based upon work supported by the National Science Foundation under Grant CHE-0808984.

References and Notes

(1) Huber, K. P.; Herzberg, G. *Constants of Diatomic Molecules*; Van Nostrand Reinhold: New York, 1979; Vol. IV.
(2) Cazzoli, G.; Cludi, L.; Puzzarini, C. *J. Mol. Struct.* **2006**, *780−781*, 260.
(3) Ahmad, I. K.; Hamilton, P. A. *J. Mol. Spectrosc.* **1995**, *169*, 286.
(4) Ghosh, S. N.; Verma, R. D.; VanderLinde, J. *Can. J. Phys* **1981**, *59*, 1640.
(5) Femelat, B.; Jones, W. E. *J. Mol. Spectrosc.* **1974**, *49*, 388.
(6) Jones, W. E. *J. Mol. Spectrosc.* **1970**, *34*, 320.
(7) Cooke, S. A.; Gerry, M. C. L. *Phys. Chem. Chem. Phys.* **2004**, *6*, 4579.
(8) Jenouvrier, A.; Daumont, D.; Pascat, B. *Can. J. Phys.* **1978**, *56*, 30.
(9) Ciach, S.; Thistlethwaite, P. J. *J. Chem. Phys.* **1970**, *53*, 3381.
(10) Cooke, S. A.; Michaud, J. M.; Gerry, M. C. L. *J. Mol. Struct.* **2004**, *695−696*, 413.
(11) Shestakov, O.; Fink, E. H. *Chem. Phys. Lett.* **1993**, *211*, 473.
(12) Harding, L.; Jones, W. E.; Yee, K. K. *Can. J. Phys.* **1970**, *48*, 2842.
(13) Yee, K. K.; Jones, W. E. *J. Chem. Soc. D* **1969**, 586.
(14) Jones, W. E.; Flinn, C. G.; Yee, K. K. *J. Mol. Spectrosc.* **1974**, *52*, 344.
(15) Breidohr, R.; Shestakov, O.; Setzer, K. D.; Fink, E. H. *J. Mol. Spectrosc.* **1995**, *172*, 369.
(16) Breidohr, R.; Shestakov, O.; Fink, E. H. *J. Mol. Spectrosc.* **1994**, *168*, 126.
(17) Thrush, B. A. *Proc. R. Soc. A* **1956**, *235*, 143.
(18) Dyke, J. M.; Jonathan, N. B. H.; Lewis, A. E.; Morris, A. *Mol. Phys.* **1982**, *47*, 1231.
(19) Brazier, C. R.; Bernath, P. F.; Burkholder, J. B.; Howard, C. J. *J. Chem. Phys.* **1988**, *89*, 1762.
(20) Pahnke, R.; Ashworth, S. H.; Brown, J. M. *Chem. Phys. Lett.* **1988**, *147*, 179.
(21) Continetti, R. E.; Cyr, D. R.; Metz, R. B.; Neumark, D. M. *Chem. Phys. Lett.* **1991**, *182*, 406.
(22) Choi, H.; Park, C.; Baeck, K. K. *J. Phys. Chem. A* **2002**, *106*, 5177.
(23) Balasubramanian, K.; Sumathi, K.; Dai, D. *J. Chem. Phys.* **1991**, *95*, 3494.
(24) Andrews, L.; Mielke, Z. *J. Phys. Chem.* **1990**, *94*, 2348.
(25) Jones, R. O.; Gantefoer, G.; Hunsicker, S.; Pieperhoff, P. *J. Chem. Phys.* **1995**, *103*, 9549.
(26) Lippa, T. P.; Xu, S. J.; Lyapustina, S. A.; Nilles, J. M.; Bowen, K. H. *J. Chem. Phys.* **1998**, *109*, 10727.
(27) Polak, M. L.; Gerber, G.; Ho, J.; Lineberger, W. C. *J. Chem. Phys.* **1992**, *97*, 8990.
(28) Gausa, M.; Kaschner, R.; Seifert, G.; Faehrmann, J. H.; Lutz, H. O.; Meiwes-Broer, K. H. *J. Chem. Phys.* **1996**, *104*, 9719.
(29) Polak, M. L.; Ho, J.; Gerber, G.; Lineberger, W. C. *J. Chem. Phys.* **1991**, *95*, 3053.
(30) Ostmark, H.; Wallin, S.; Hore, N.; Launila, O. *J. Chem. Phys.* **2003**, *119*, 5918.
(31) Kornath, A.; Kaufmann, A.; Torheyden, M. *J. Chem. Phys.* **2002**, *116*, 3323.
(32) Boudon, V.; Mkadmi, E. B.; Burger, H.; Pierre, G. *Chem. Phys. Lett.* **1999**, *305*, 21.
(33) Brassington, N. J.; Edwards, H. G. M.; Long, D. A. *J. Raman Spectrosc.* **1981**, *11*, 346.
(34) Eiduss, J.; Chikvaidze, G.; Kalendarev, R.; Rodionov, A.; Sazonov, A. *J. Mol. Struct.* **1995**, *348*, 123.
(35) Killeen, K. P. *J. Appl. Phys.* **1993**, *73*, 2596.
(36) Bosworth, Y. M.; Clark, R. J. H.; Rippon, D. M. *J. Mol. Spectrosc.* **1973**, *46*, 240.
(37) Brumbach, S. B.; Rosenblatt, G. M. *J. Chem. Phys.* **1972**, *56*, 3110.
(38) Dyke, J. M.; Morris, A.; Stevens, J. C. H. *Chem. Phys.* **1986**, *102*, 29.
(39) Elbel, S.; Kudnig, J.; Grodzicki, M.; Lempka, H. J. *Chem. Phys. Lett.* **1984**, *109*, 312.
(40) Teichman, R. A., III.; Nixon, E. R. *J. Chem. Phys.* **1977**, *67*, 2470.
(41) Bondybey, V. E.; English, J. H. *J. Chem. Phys.* **1980**, *73*, 42.
(42) Bondybey, V. E.; Schwartz, G. P.; Griffiths, J. E.; English, J. H. *Chem. Phys. Lett.* **1980**, *76*, 30.
(43) Ahmed, F.; Nixon, E. R. *J. Chem. Phys.* **1981**, *75*, 110.
(44) Eberle, B.; Sontag, H.; Weber, R. *Chem. Phys.* **1985**, *92*, 417.
(45) Desclaux, J. P. *At. Data Nucl. Data Tables* **1973**, *12*, 311.

(46) Cotton, F. A.; Wilkinson, G. *Advanced Inorganic Chemistry*, 3rd ed.; Wiley: New York, 1972.
(47) Condon, E. U.; Shortley, G. H. *The Theory of Atomic Spectra*, 2nd ed.; University Press: Cambridge, 1970.
(48) Lefebvre-Brion, H.; Field, R. W. *Perturbations in the Spectra of Diatomic Molecules*, 1st ed.; Academic Press: Orlando, FL, 1986.
(49) Fu, Z.; Lemire, G. W.; Hamrick, Y. M.; Taylor, S.; Shui, J.-C.; Morse, M. D. *J. Chem. Phys.* **1988**, *88*, 3524.
(50) Wiley, W. C.; McLaren, I. H. *Rev. Sci. Instrum.* **1955**, *26*, 1150.
(51) Karataev, V. I.; Mamyrin, B. A.; Shmikk, D. V. *Zh. Tekh. Fiz.* **1971**, *41*, 1498.
(52) Mamyrin, B. A.; Karataev, V. I.; Shmikk, D. V.; Zagulin, V. A. *Zh. Eksp. Teor. Fiz.* **1973**, *64*, 82.
(53) Yoo, R. K.; Ruscic, B.; Berkowitz, J. *J. Electron Spectrosc. Relat. Phenom.* **1993**, *66*, 39.
(54) Loree, T. R.; Sze, R. C.; Barker, D. L. *Appl. Phys. Lett.* **1977**, *31*, 37.
(55) Wilke, V.; Schmidt, W. *Appl. Phys.* **1978**, *16*, 151.
(56) Clouthier, D. J.; Karolczak, J. *Rev. Sci. Instrum.* **1990**, *61*, 1607.
(57) Gerstenkorn, S.; Luc, P. *Atlas du Spectre d'Absorption de la Molécule d'Iode entre 14 800−20 000 cm^{-1}*; CNRS: Paris, 1978.
(58) Gerstenkorn, S.; Luc, P. *Rev. Phys. Appl.* **1979**, *14*, 791.
(59) Bevington, P. R. *Data Reduction and Error Analysis for the Physical Sciences*; McGraw-Hill: New York, 1969.
(60) Herzberg, G. *Molecular Spectra and Molecular Structure III. Electronic Spectra and Electronic Structure of Polyatomic Molecules*; Van Nostrand Reinhold: New York, 1966.
(61) Manzel, K.; Engelhardt, U.; Abe, H.; Schulze, W.; Froben, F. W. *Chem. Phys. Lett.* **1981**, *77*, 514.
(62) Behm, J. M.; Arrington, C. A.; Langenberg, J. D.; Morse, M. D. *J. Chem. Phys.* **1993**, *99*, 6394.
(63) Behm, J. M.; Arrington, C. A.; Morse, M. D. *J. Chem. Phys.* **1993**, *99*, 6409.
(64) Wheeler, R. G.; Laihing, K.; Wilson, W. L.; Duncan, M. A. *Chem. Phys. Lett.* **1986**, *131*, 8.
(65) Walstedt, R. E.; Bell, R. F. *J. Chem. Phys.* **1987**, *87*, 1423.
(66) Mathews, C. W.; Ginter, M. L.; Ginter, D. S.; Brown, C. M. *J. Opt. Soc. Am. B* **1989**, *6*, 1627.
(67) Moore, C. E. *Atomic Energy Levels*; National Bureau of Standards, U.S. Circ. No. 467 ed.; U.S. Government Printing Office: Washington, D.C., 1971.
(68) Lefebvre-Brion, H.; Field, R. W. *The Spectra and Dynamics of Diatomic Molecules*; Elsevier: Amsterdam, 2004.
(69) Ishiguro, E.; Kobori, M. *J. Phys. Soc. Jpn.* **1967**, *22*, 263.
(70) Barckholtz, T. A.; Miller, T. A. *Int. Rev. Phys. Chem.* **1998**, *17*, 435.
(71) Sioutis, I.; Stakhursky, V. L.; Pitzer, R. M.; Miller, T. A. *J. Chem. Phys.* **2007**, *126*, 124308/1.
(72) Sioutis, I.; Stakhursky, V. L.; Pitzer, R. M.; Miller, T. A. *J. Chem. Phys.* **2007**, *126*, 124309/1.

JP806436N